Journal of Environmental Management 322 (2022) 116001

Contents lists available at ScienceDirect

Journal of Environmental Management

journal homepage: www.elsevier.com/locate/jenvman

Research article

Detecting the causal influence of thermal environments among climate regions in the United States

Xueli Yang [a], Zhi-Hua Wang [a,*], Chenghao Wang [b], Ying-Cheng Lai [c,d]

[a] School of Sustainable Engineering and the Built Environment, Arizona State University, Tempe, AZ, 85287, USA
[b] Department of Earth System Science, Stanford University, Stanford, CA, 94305, USA
[c] School of Electricity, Computer and Energy Engineering, Arizona State University, Tempe, AZ, 85287, USA
[d] Department of Physics, Arizona State University, Tempe, AZ, 85287, USA

ARTICLE INFO

Keywords:
Causality
Complex network
Convergent cross mapping
System dynamics
Thermal environment

ABSTRACT

The quantification of cross-regional interactions for the atmospheric transport processes is of crucial importance to improve the predictive capacity of climatic and environmental system modeling. The dynamic interactions in these complex systems are often nonlinear and non-separable, making conventional approaches of causal inference, such as statistical correlation or Granger causality, infeasible or ineffective. In this study, we applied an advanced approach, based on the convergent cross mapping algorithm, to detect and quantify the causal influence among different climate regions in the contiguous U.S. in response to temperature perturbations using the long-term (1901–2018) climatology of near surface air temperature record. Our results show that the directed causal network constructed by convergent cross mapping algorithm, enables us to distinguish the causal links from *spurious* ones rendered by statistical correlation. We also find that the Ohio Valley region, as an atmospheric convergent zone, acts as the regional gateway and mediator to the long-term thermal environments in the U.S. In addition, the temporal evolution of dynamic causality of temperature exhibits superposition of periodicities at various time scales, highlighting the impact of prominent low frequency climate variabilities such as El Niño–Southern Oscillation. The proposed method in this work will help to promote novel system-based and data-driven framework in studying the integrated environmental system dynamics.

1. Introduction

The Earth's environment and climate systems involve complex dynamic processes that are non-separable, interacting, and more importantly, having causal influences toward one another. Prominent examples include the drought patterns in the western U.S. that are strongly regulated by the sea surface temperature (SST) of the Pacific (Namias, 1983), the long-distant links (aka teleconnections) between ground level temperature and atmospheric Rossby waves (Wang et al., 2013), the correlation between anomalous atmospheric circulation and sea ice concentration (Handorf et al., 2015), to name a few. Conventionally, the spatial or inter-variable correlations in the climate system has been established by statistical regression of observational time series or dissimilarity functions via information transfer (e.g., Moran, 1953; Fitzpatrick and Dunn, 2019; Wang et al., 2020a).

On the other hand, successful identification of the directed dynamical influence, viz. *causality*, in Earth's climate system will greatly enhance the modeling and predictive capacity of physically based Earth modeling frameworks (Runge et al., 2015, 2019; Jiang et al., 2016; Leng et al., 2020; Huang et al., 2021). However, the conventional statistical correlation-based methods to infer causality may induce *spurious* links that correlate climate variables driven by the same external forcing but without mutual causal influence (Moran, 1953). These ephemeral or "mirage" correlations (false causality) are common in nonlinear systems. Their presence can lead to incorrect and even contradictory hypotheses (Sugihara et al., 2012), which can impede our understanding of true interactions among system dynamics. In particular, inferring causality from statistical correlation is risky for the Earth's climate system that involves nonlinear dynamics with weak and moderate interactions (McCann et al., 1998). The nonlinearity of climate dynamics, especially the temperature evolution, has been extensively studied in response to, e.g. different CO_2 emission scenarios (Good et al., 2015), which is largely attributed to the nonlinear albedo feedback such as the sea-ice albedo feedbacks (Hall, 2004; Ishizaki et al., 2012). Furthermore, our

* Corresponding author.
E-mail address: zhwang@asu.edu (Z.-H. Wang).

https://doi.org/10.1016/j.jenvman.2022.116001
Received 6 May 2022; Received in revised form 7 August 2022; Accepted 10 August 2022
Available online 26 August 2022

previous analysis of long-term temperature anomalies show that the time series exhibit significant increase in autocorrelation and variance prior to critical transitions that features nonlinear dynamic systems (Wang et al., 2020b).

In the literature, the Granger causality (GC) scheme has been commonly used for causal inference, with the key assumption that a variable is causative to a dynamic system if the prediction skill increases by adding this variable to the system's autoregressive processes (Granger, 1969). GC analysis has been applied to climate sciences, examples including the potential causality between El Niño–Southern Oscillation (ENSO) and temperature and wind patterns across the mid-to-high latitudes (McGraw and Barnes, 2018). More recently, Silva et al. (2021) identified GC-based climate teleconnections between the precipitation response to SST and ENSO. Nevertheless, there are some intrinsic disadvantages in GC-based causality analysis, especially the requirement of strong coupling and separability of system dynamics. These assumptions often lead to the loss of feasibility of GC's causality inference, especially in the Earth's climate system where nonlinearity, weakly or moderately coupled dynamics, and nonseparability prevail (Ancona et al., 2004). To overcome the inherited limitation of the GC approach, Sugihara et al. (2012) developed a new method of causal inference based on the convergent cross mapping (CCM) algorithm. The CCM method and its variations (e.g. partial cross mapping, see Runge et al., 2015; Leng et al., 2020) have been successfully applied to detect dynamic causality in Earth's climate system, such as the causal influence of greenhouse gas concentration and midlatitude circulation on global climate changes (van Nes et al., 2015), and the detection of atmospheric teleconnections in monsoon dynamics (Runge et al., 2015). In addition, causal inference methods have been evaluated in the study of hydrometeorological systems (Wang et al., 2018; Ombadi et al., 2020). In particular, Shi et al. (2022) proposed a new perspective to use causality to detect the drought propagation, in contrast to the overuse of correlation analysis.

In this study, we apply the CCM method to quantify the causal influence in temperature perturbations among different climate regions in the contiguous U.S. (CONUS), using the long-term temperature climatology in 1901–2018. The detection of cross-regional causal interactions can provide new insights to understanding the response of thermal environments (and associated atmospheric transport) to emergent anomalous climatic patterns, with implications to occurrence of extreme events such as mega-heatwaves or persistent droughts. Our analysis also enables us to identify key climate regions, viz. mediators, as critical atmospheric gateways in spreading and distributing climate perturbations, by constructing the CONUS climate system as a complex network. The construction of the causal network, in turn, will facilitate the imperative need of the development of data-driven and system-based frameworks in the integrated Earth system (Fan et al., 2020; Wang and Wang, 2020; Wang, 2021, 2022).

2. Methods

2.1. Data retrieval and treatment

In this study, we retrieved the monthly mean near-surface temperature over the period 1901–2018 from Climatic Research Unit (CRU) Time-Series (TS) version 4.03 (https://catalogue.ceda.ac.uk/uuid/10d3e3640f004c578403419aac167d82) produced by the Center for Environmental Data Analysis (CEDA) Archive. The 0.5° × 0.5° spatially gridded dataset covers the spatial domain of global land surfaces except Antarctica, with a total number of 3288 grid cells over the entire CONUS. The observational data are anomalized using 1961–1990 monthly averages for each grid cell (Harris et al., 2020). We aggregated all CONUS grid cells into nine climatic regions, to better represent the thermal environments in individual regions with distinct background climatic and geographic conditions. These climatic regions are Northwest (NW), West (WE), Southwest (SW), Northern Rockies and Plains (NRP), South (SO), Upper Midwest (UM), Ohio Valley (OV), Southeast (SE), and Northeast (NE). The division of climate regions is defined by the National Centers for Environmental Information of NOAA (https://www.ncdc.noaa.gov/monitoring-references/maps/us-climate-regions.php). We then removed the seasonal cycle by subtracting monthly anomalies averages from the regional temperature anomalies time series during the study period to minimize the impact of seasonality. The detrended time series of temperature anomalies are used for subsequent causality analysis.

2.2. The convergent cross-mapping CCM method to estimate causality

The CCM method has been developed to detect and quantify the directed causal influence among key parameters in nonlinear dynamic systems, based on the embedding theory (Sugihara et al., 2012). The fundamental concept of the CCM algorithm is that if causality exists between a pair of generic variables, represented by vectors (adequately long time series) X and Y, then we can reconstruct the cross-mapping dynamics of one variable from the information of the other. The reconstruction of phase space for each dynamical variable is based on the delay-coordinate embedding method (Takens, 1981). In addition, CCM uses simple projection (Sugihara & May 1990), i.e. a nearest-neighbor algorithm that involves exponentially weighted distances from nearby points on a reconstructed manifold, to make kernel estimation.

For a dynamically coupled canonical Lorenz system, the CCM algorithm is illustrated in Fig. 1, where the reconstructed lagged-coordinate vector for time series $X(t)$ with length L is denoted as $\boldsymbol{x}(t) = [X(t), X(t-\tau), \ldots, X(t-(E-1)\tau)]$, with τ and E the time delay and embedding dimension to construct the shadow manifold M_X, respectively (likewise for $\boldsymbol{y}(t)$ and M_Y). The embedding dimension E can be physically interpreted as the complexity of the state variable (in our case, temperature) as to be causally influenced by other confounding variables in the complex system. For example, it is found that causal analysis of precipitation requires a much larger embedding dimension that of temperature, indicating the physics of precipitation is of higher complexity than that of heat transfer. In addition, the time delay $\tau = 1$ is equivalent to use consecutive data points in the data series (without filtering) to construct shadow manifolds based on the delay-coordinate embedding. The shadow manifold, constructed using these parameters, represents the low-dimensional approximations of the true system that could be of infinitely high dimension in theory. Thus, the convergence of the CCM method will be limited by observational error, process noise, and time-series length L, e.g. with limited or noisy field data, the predictability of CCM is demonstrated to increases with L.

If two generic variables X and Y are causally coupled in a complex system, there is a cross-mapping correspondence between the two attractor manifolds M_X and M_Y. For the given time series $Y(t)$, its cross-mapping estimate $Y(t)|M_X$ is based on a simple projection of the $E+1$ nearest neighbors of vector $\boldsymbol{x}(t)$ in the manifold of M_X, where $E+1$ is the minimum number of points required for a bounded simplex in the E-dimensional space. The time indices of those $E+1$ neighbors $\boldsymbol{x}(t_1)$, $\boldsymbol{x}(t_2)$, …, $\boldsymbol{x}(t_{E+1})$ (from closest to farthest) in M_X are used to identify the corresponding putative neighbors in Y, i.e. $Y(t_1)$, $Y(t_2)$, …, $Y(t_{E+1})$. The cross-mapping estimate of $Y(t)$, denoted as $Y(t)|M_X$, is determined using the weighted average as

$$\widehat{Y}(t)\Big|M_X = \sum_{i=1}^{E+1} w_i(t)\cdot Y(t_i), \tag{1}$$

where the weight vector $w_i(t)$ is estimated by

$$w_i(t) = \frac{u_i(t)}{\sum_{j=1}^{E+1} u_i(t)}, \tag{2}$$

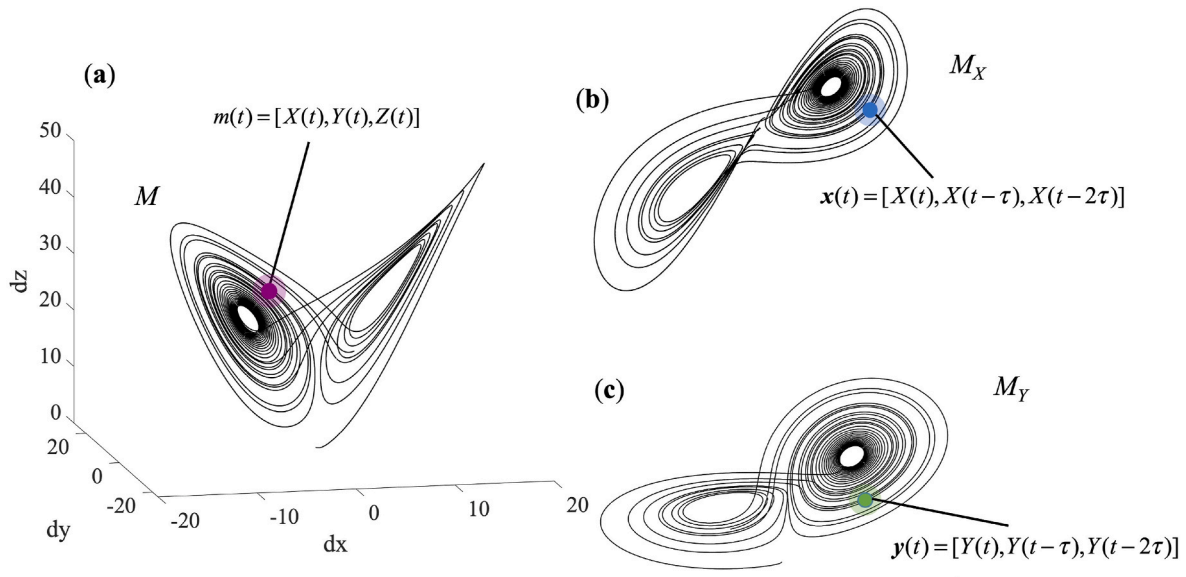

Fig. 1. Illustration of correspondence between two shadow manifolds of convergent cross mapping: (**a**) the canonical Lorenz system m with three coupled vectors X, Y, and Z, with two attractors projected onto the manifolds of (**b**) M_X and (**c**) M_Y.

with

$$u_i(t) = \exp\left\{ -\frac{d[x(t), x(t_i)]}{d[x(t), x(t_1)]} \right\}, \tag{3}$$

and $d[x(t), x(t_i)]$ the Euclidean distance between the two vectors $x(t)$ and $x(t_i)$ in M_X. To measure the causality from Y to X, the correlation coefficient $\rho_{Y|M_X}$ between the original $Y(t)$ and the cross-mapping estimate $\widehat{Y}(t)|M_X$ will be used, which is defined by

$$\rho_{Y|M_X} = \frac{\mathbf{E}\{[Y(t) - \mu_Y] \cdot [\widehat{Y}(t)|M_X - \mu_{\widehat{Y}}]\}}{\sigma_Y \sigma_{\widehat{Y}}}, \tag{4}$$

where $\mathbf{E}$, μ, and σ are the statistical expectation, average, and standard deviation, respectively. The larger value implies a stronger casual influence, while Y is not causal to X if $\rho_{Y|M_X} \leq 0$.

2.3. Time delay and embedding dimension to reconstruct phase-space dynamical system

Since the CCM method is derived from the standard delay-coordinate embedding method (Takens, 1981), the phase space of the underlying dynamical system can be reconstructed from time series and the accuracy of the reconstruction requires the proper choice of the time delay τ and the embedding dimension E. The value of the time delay can be computed as the autocorrelation length (Kantz and Schreiber, 1997). Empirically, the delay time can be chosen as the average oscillation period of the underlying times series, that is corresponding to unit value in discrete-time map (Lai and Ye, 2003; Grassberger and Procaccia, 1983, 2004). Thus, for temperature anomaly here the time delay is chosen as $\tau = 1$. The properly chosen embedding dimension E can be determined using the correlation integral and dimension method or the GP-algorithm (Grassberger and Procaccia, 1983; Lai and Ye, 2003). The correlation dimension D_2 in nonlinear time series can be evaluated by using the correlation integral $C(\varepsilon)$, which is the probability that a pair of points chosen randomly in the reconstructed phase space is within a hypersphere of radius ε (Grassberger and Procaccia, 1983; Lai and Ye, 2003). For the reconstructed vector time series $\boldsymbol{x}(t)$ with number of points N inside, the correlation integral can be approximated by

$$C_N(\varepsilon) = \frac{1}{N(N-1)} \sum_{j=1}^{N} \sum_{i=j+1}^{N} \Theta\left(\varepsilon - \|\boldsymbol{x}_i - \boldsymbol{x}_j\|\right), \tag{5}$$

where Θ is the Heaviside step function, and $\|\boldsymbol{x}_i - \boldsymbol{x}_j\|$ is the distance between $\boldsymbol{x}_i$ and $\boldsymbol{x}_j$. The correlation dimension D_2 is given by consequently

$$D_2 = \lim_{\varepsilon \to 0} \lim_{N \to \infty} \frac{\log C_N(\varepsilon)}{\log \varepsilon}. \tag{6}$$

In practice, the correlation dimension D_2 is estimated by examining the slope of the linear portion of $\log C_N(\varepsilon)$ versus $\log\varepsilon$ for a series of increasing values of m (different embedding dimensions). Results of detailed calculations of the correlation integrals and correlation dimension from the aggregated time series of temperature anomalies are shown in Fig. 2. The slope in the plot increases with m until it reaches a plateau and the slope value at the plateau is then taken as the D_2 estimation (Grassberger and Procaccia, 1983; Ding et al., 1993). The results show the D_2 estimation is around 1.7, the embedding dimension E for the reconstruction must be sufficiently large as for an infinite, noiseless time series, the estimated dimension value D_2 increases with E but plateaus for $E > [\overline{D_2}] + 1$ (Ding et al., 1993), so the embedding dimension is determined as $E = 3$.

2.4. The regional causal effect and causal susceptibility

The aforementioned algorithm enables us to quantify the directed causality between the temperature anomalies in each pair of climate regions, resulted in a directed causal *network* of temperature climatology in CONUS with nine nodes, each representing one climate region. Using this network, we define two indices to measure the causal effect and causal sensitivity for a climate region: the average causal *effect* (*ACE*) and the average causal *susceptibility* (*ACS*). The estimate of *ACE* and *ACS* for a given region R can be calculated by averaging along individual column and rows of the adjacency matrix of the causality network, respectively (Runge et al., 2015):

$$ACE_R(t) = \frac{1}{N_R - 1} \sum_{i \neq R} \rho_{X_R(t)|M_i}, \tag{7}$$

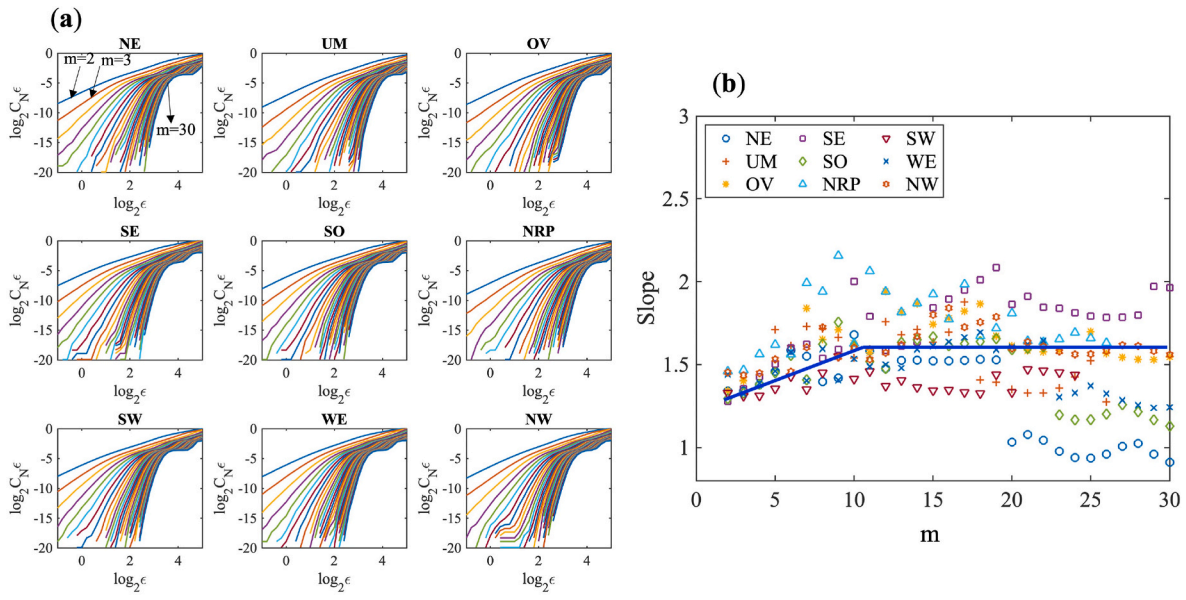

Fig. 2. Determination of the embedding dimension E using the GP-algorithm of correlation integral and dimension from the aggregated time series of regional temperature anomalies: (**a**) plots of the correlation integral on a logarithm scale for different embedding dimension $m = 1, \ldots, 30$ for the nine climate regions, and (**b**) the slope values of $\log C_N(\varepsilon)$ versus $\log\varepsilon$ for the nine climate regions obtained from a least-squares fitting. The slope increases with m and reaches an approximate plateau value, as shown by the two blue solid lines for eye guidance. (For interpretation of the references to color in this figure legend, the reader is referred to the Web version of this article.)

$$ACS_R(t) = \frac{1}{N_R - 1}\sum_{i \neq R} \rho_{X_i(t)|M_R}, \tag{8}$$

where N_R is the total number of climate regions. Furthermore, to investigate the long-term trend of *ACE* and *ACS*, we compute their running averages using a sliding window of size w, as for a time window [k-(w-1)/2, k+(w-1)/2], with k at the middle of the time window, as

$$\overline{ACE}_{R,k} = \frac{1}{w}\sum_{j=k-(w-1)/2}^{k+(w-1)/2} ACE(j), \tag{9}$$

$$\overline{ACS}_{R,k} = \frac{1}{w}\sum_{j=k-(w-1)/2}^{k+(w-1)/2} ACS(j). \tag{10}$$

In a given region R, a larger *ACE* value means a stronger causal effect of that region to mediate the thermal climatology in other regions. Likewise, a higher *ACS* value signifies that the region is more susceptible to thermal perturbations of other regions.

3. Results and discussion

3.1. Statistical correlation vs. causality

We first constructed a directed causal network of the temperature climatology among the nine CONUS climatic regions, using the CCM algorithm outlined in Section 2. The inter-regional interactions of climatic variables have been quantified using conventional statistical similarity functions or Granger causality methods that directly link the time series of climatic variables between a pair of nodes (Boers et al., 2019; Fitzpatrick and Dunn, 2019; Silva et al., 2021). In this study, in addition to CCM analysis, we also constructed an *undirected* CONUS regional network using statistical correlation coefficient, defined in Eq. (4) but between the observed $X(t)$ (instead of cross-mapping estimate) and $Y(t)$ directly.

Fig. 3 shows the comparison of the undirected correlation (Fig. 3**a**) and directed causality (Fig. 3**b**) networks. It is noteworthy that the network of statistical correlations is stronger than the causal counterpart, as manifested by the darker color in Fig. 3**a** representing higher strength. By definition, the correlation network is symmetric and without directionality. In comparison, the directed causal network is generally asymmetric, as the causal influence from X to Y is not necessarily the same as that from Y to X. In this specific case, however, the causality network of CONUS temperature climatology (Fig. 3**b**) is rather (not completely though) symmetric, suggesting the cross-regional causal influence among CONUS climate regions is, in general, reciprocated in terms of the atmospheric heat transfer. For example, the temperature in the OV region exerts a causal influence on four neighboring regions (NE, UM, SE, SO) with strength greater than 0.6, while the latter regions responded with a mutual causal effect with comparable strength. The cause-effect network of temperature in Fig. 3**b** is sparser (with less number of connectivities) than the one from the simple correlations in Fig. 3**a**, because the latter often admits spurious links due to common external variables (Shi et al., 2022; Sugihara et al., 2012).

To facilitate a more direct comparison of the statistical correlation and causality, we identified the effect links in the networks using a common threshold value of 0.5. The choice of this threshold is adopted from the suggested value by previous studies (Tsonis and Roebber, 2004; Yang et al., 2022), which has been tested to be statistically significant. A pair of climate regions is considered as effectively connected (statistically or causally) if the strength in matrices of Fig. 3**a** and **b** is greater than 0.5. The choice of this threshold value follows previous study of thermal climate network and was validated by statistical test (Tsonis and Roebber, 2004; Wang et al., 2021). The results are shown in Fig. 3**c**, where the links with significant statistical correlation but no causality are marked as *spurious* links and represented by gray dash lines. In this case, we identified three spurious links, namely that connect SW and NRP, SW and SO, and SO and UM.

The number of spurious links is seemingly small, but the implication is significant. First, the South and Southwest regions stand out as most significantly affected by spurious links, likely due to the analogy in thermal environments that subject to common radiative forcing. Secondly, by removing the spurious links in Fig. 3**c**, the southern part of the CONUS thermal climate network is effectively a bipartite system with distinct east and west clusters. The emergence of clustering in CONUS climate network is consistent with the finding in a previous study based

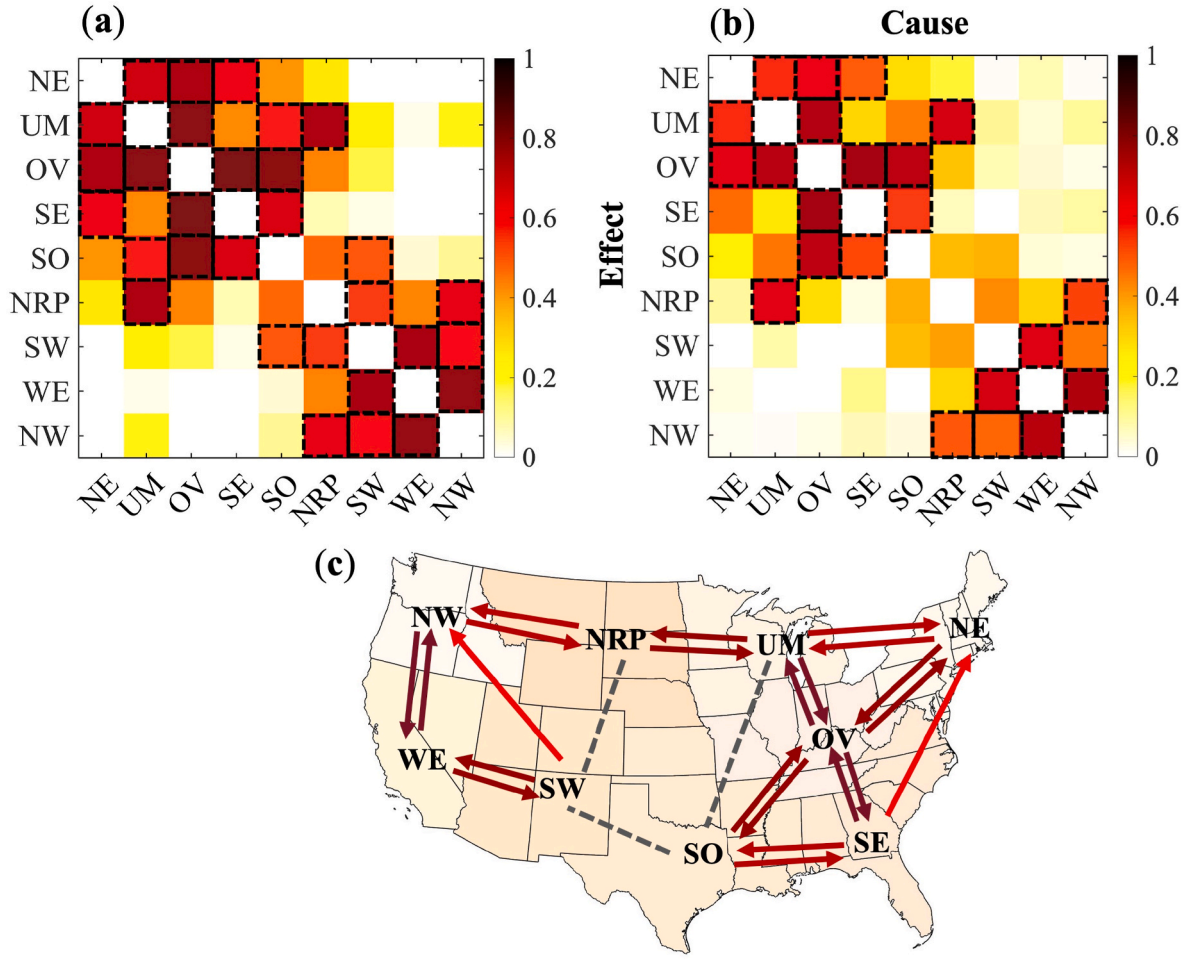

Fig. 3. Comparison of the correlation and causality networks for the nine CONUS climate regions: (**a**) the matrix of connectivity determined by undirected statistical correlation, (**b**) the matrix of connectivity determined by directed causality, and (**c**) graphic representation of causal and spurious links resulted from (**a**) and (**b**), with a threshold strength of 0.5. Cells with dashed boxes in (**a**) and (**b**) represent causally (above the threshold) connected pairs. The gray dashed lines represent the spurious link between different regions, and lines with an arrow the directed causal influence with strength denoted by different colors (the same scale as in (**b**)). (For interpretation of the references to color in this figure legend, the reader is referred to the Web version of this article.)

on advanced information theory (Wang et al., 2020a). More specifically, in the east half of the CONUS network, the Ohio Valley region appears to be the gateway of cross-regional thermal interactions. This is not only due to the geographic location of the region, but also agrees with climatic observations and modeling results as reported in the literature as well (detailed below in Section *3.2*).

In addition, we also constructed the causal graphs using the GC approach. The results are shown in Figs. A1 and A2 in Appendix. It can be seen that the causality networks detected by GC, though self-consistent, are at variance with and not comparable to those detected by CCM or conventional statistical correlation (Fig. 3a and b). This discrepancy can be attributed to that the GC method is: (1) not most fitful for nonlinear systems with moderate coupling, and (2) very sensitive to the choice of maximum delay τ_{max} to do the autoregression analysis, the determination of which can be rather arbitrary and does not admit a solid physical interpretation.

3.2. Regional causal effect and susceptibility

We then further investigate the causal network and quantify the role of each climate region in transporting and distributing temperature perturbations. It was found that regions with strong strength in causal effect and/or susceptibility are linked with major atmospheric uplifting zones in complex climate systems (Runge et al., 2015). The results of calculated *ACE* and *ACS* indices, as defined in Eqs. (7) and (8) and averaged over the entire study period, are shown in Fig. 4, mapped over CONUS. It is clear that the Ohio Valley region acts as a causal gateway and mediator at the same time, manifested as the brightest region (i.e. with highest values of *ACE* and *ACS*). This means that the Ohio Valley is the most conducive to spreading temperature anomalies (e.g. heat extremes) to (Fig. 4**a**), meanwhile the most susceptible to thermal perturbations arising from (Fig. 4**b**) other regions in CONUS. Potential physical mechanisms that contribute to making OV a regional gateway include: (a) this region has the strongest geostrophic wind components (Walsh et al., 1982); (b) it is most significantly affected by ENSO and temperature extremes (Gershunov and Barnett, 1998); and (c) it mediates atmospheric heat transfer and drought distribution in the U.S. with high climate variability (Karl and Koscielny, 1982; Konapala and Mishra, 2017; Zhang et al., 2010).

In the western U.S., the NW, WE, and SW regions, in general, have weaker local causal influence than their eastern counterparts. Nevertheless, due to the presence of long-range connectivity among CONUS climate regions, the susceptibility of the Great Plains to climatic extremes, e.g. summer drought and heatwaves, could also be regulated by the Pacific oceanic conditions. For example, Namias (1983) found that in the West, the local surface circulation is characterized by easterly wind anomalies that are originated from the continental interior and mostly directed down the slope of the Rocky Mountain Ridge (Lau and Nath, 2012). The western ridges therefore contribute to build *blocking* high pressure systems to cyclonic activity from the Pacific. As a

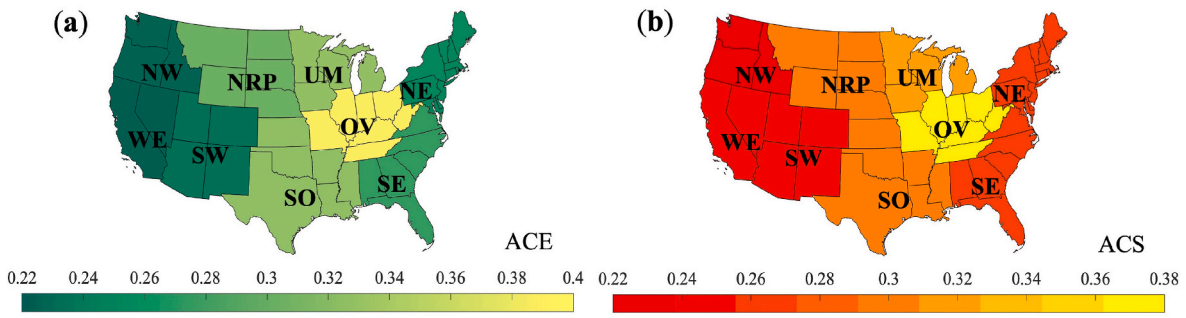

Fig. 4. Quantification of (**a**) the average causal effect and (**b**) the average causal susceptibility for the temperature climatology in CONUS. The colors correspond to the causal effect or susceptibility strength. (For interpretation of the references to color in this figure legend, the reader is referred to the Web version of this article.)

consequence, the development of a North Pacific oscillation (NPO) exerts a causally dynamic influence on the atmospheric transport of heat and moisture, in particular storm tracks, as to amplify and stabilize the heat and drought patterns (Charney and DeVore, 1979; Namias, 1983; Matsueda, 2011). This causal influence in climate dynamics is largely responsible for the persistent drought and mega-heatwave episodes over the western U.S. in summers (Perkins, 2015; Wang et al., 2021).

3.3. Temporal variability and periodicity of causality

The dynamics of complex climate system are known to subject to temporal variability ranging from seasonal to millennium time scales (Kenyon and Hegerl, 2008; Ghil and Lucarini, 2020), so does their causal influence. In this study, we further attempt to look into the temporal variability and the presence of possible periodicity in the causal network of CONUS temperature anomalies, by looking into the running means of *ACE* and *ACS* defined in Eqs. (9) and (10). The results are shown in Fig. 5, with a 15-year sliding window size. The time evolution of *ACE* and *ACS* in all the nine climate regions exhibit patterns of superposition of climatic periodicity at different time scales, as expected. The low frequency climatic variability at decadal scale is discernible in the time history, which are likely due to the influence of ENSO or NPO as their influence is manifested in determining the atmospheric gateways as discussed before (Section 3.2). In particular, the strong correlation between ENSO and the general trend of global temperature changes has been well demonstrated (e.g. Arblaster and Alexander, 2012). It was also found that the Pacific Decadal Oscillation (PDO) has great impacts on the temperature extremes over the northern Pacific Rim and North America (Kenyon and Hegerl, 2008). In addition, it has been tantalizingly suggested that the presence of persistent droughts and heat over

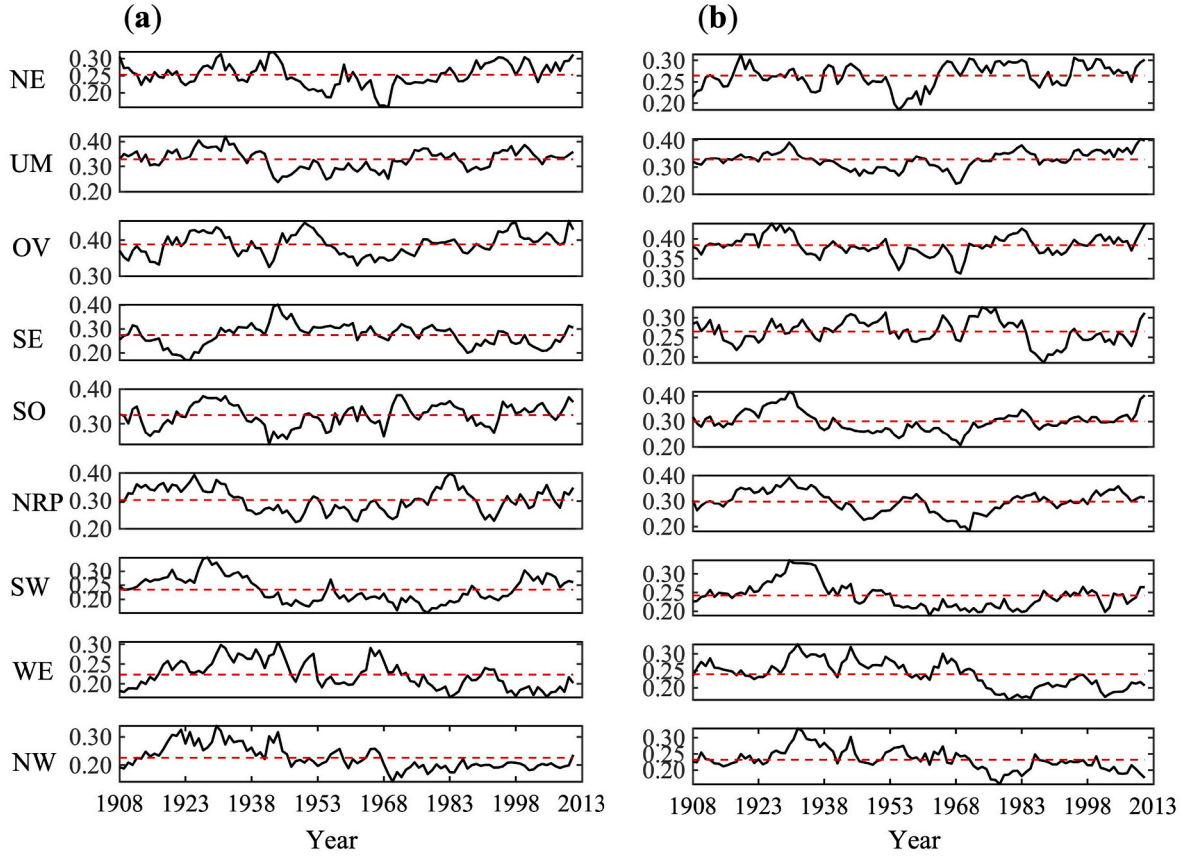

Fig. 5. Temporal evolution of the running means of (**a**) *ACE* and (**b**) *ACS* of the causal network for CONUS regional temperature anomalies. A 15-year sliding window size is used, with the red dashed lines denoting the mean values over the entire study period. (For interpretation of the references to color in this figure legend, the reader is referred to the Web version of this article.)

the western U.S. may be linked to the double sunspot cycle, with a periodicity of re-occurrence around 20–25 year (Namias, 1983). The western high pressure may be periodically reinforced by downstream strong cyclonic systems from central and eastern North America, and the characteristics of the regional pressure may contribute to the temperature periodicity in western US (Namias, 1983). In the Great Plains region, the low-frequency circulation changes suggest that there exists a prominent mid-tropospheric blocking anticyclone over that region, and these air patterns are in a realignment with the planetary-scale wave structure (Lau and Nath, 2012).

These aforementioned mechanisms of climatic periodicity were, in the literature, mostly observed or explained as statistical correlations, while their causal influence remain obscure up to date. The results in Fig. 5 provide some clue to further unravel the *causal* dynamics in the CONUS climate system. Other than the natural climate variability, the periodicity or cyclicity of causal dynamics has been under-explored up to date. To fully disentangle the various principal modes of the causal variability, it requires further spectral analysis using more sophisticated tools, such as the empirical mode decomposition (EMD) analysis (Huang et al., 1998).

4. Concluding remarks

The spreading of thermal perturbations dictates the atmospheric heat transfer in the Earth system. The data-driven causal inference method, i.e. the CCM algorithm, provides new insights to identify thermal influence and feedback among the climate regions in CONUS, using the long-term near surface air temperature observations. Our results demonstrate that the conventional statistical method to infer causal relationships may lead to *spurious* links in Earth's climate system that is moderately coupled. As indicated by the directed causal network, our findings highlight the Ohio Valley as the regional thermal mediator to the temperature perturbations over the CONUS. It is noteworthy that the CCM method can be applied to identify causal relationship between different variables that also contribute to regulating the thermal environment of the U.S., e.g. pressure, wind, soil moisture, *etc*. Introducing these confounding variables in the causal analysis will enable us to construct more informative (and more complex) causal graphs that vary spatio-temporally and cross pairwise variable. Nevertheless, disentangling and interpretating information in such complex causal graphs present physical and numerical challenges that need to be tackled in future studies; one example of such challenge will be on how to determine the cross-variable embedding dimension E in the CCM method. In future studies, it is important to extend the proposed method to investigate the key role that the major climate oscillations play behind the causality of thermal interactions, and to better understand the physical mechanisms in the occurrence of extreme events such as heatwaves and persistent droughts.

Credit Author Statement

Xueli Yang: Methodology, Software, Validation, Data curation, Writing- Original draft, Writing- Review & Editing, Visualization **Zhi-Hua Wang**: Conceptualization, Methodology, Resources, Writing-Original draft, Writing- Review & Editing, Supervision, Funding acquisition **Chenghao Wang**: Data curation, Software, Writing- Review & Editing **Ying-Ching Lai**: Conceptualization, Methodology, Writing-Review & Editing.

Declaration of competing interest

The authors declare that they have no known competing financial interests or personal relationships that could have appeared to influence the work reported in this paper.

Data availability

The authors do not have permission to share data.

Acknowledgements

This study is based upon work supported by the U.S. National Science Foundation (NSF) under Grants # AGS-1930629 and CBET-2028868, and the National Aeronautics and Space Administrations (NASA) under Grant No. 80NSSC20K1263. YCL acknowledges the support by the Office of Naval Research under Grant No. N00014-21-1-2323. The authors thank the Associate Editor Dr. Zhiyuan Cong and two anonymous reviewers for their constructive feedback for improving the quality of the paper.

Appendix

.

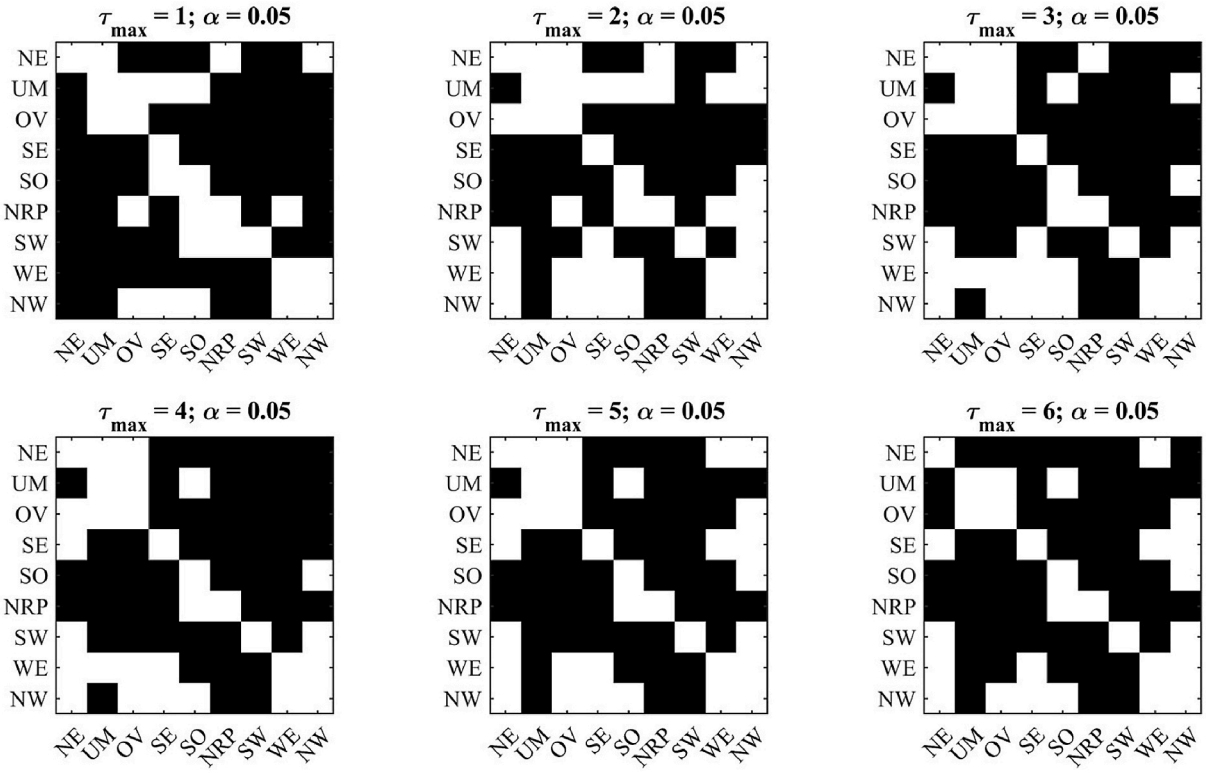

Fig. A1. The temperature interactions among the CONUS using Granger Causality method, where τ_{max} is the maximum time delay of the GC autoregression model, and α the significance level. The black cells represent effective causality.

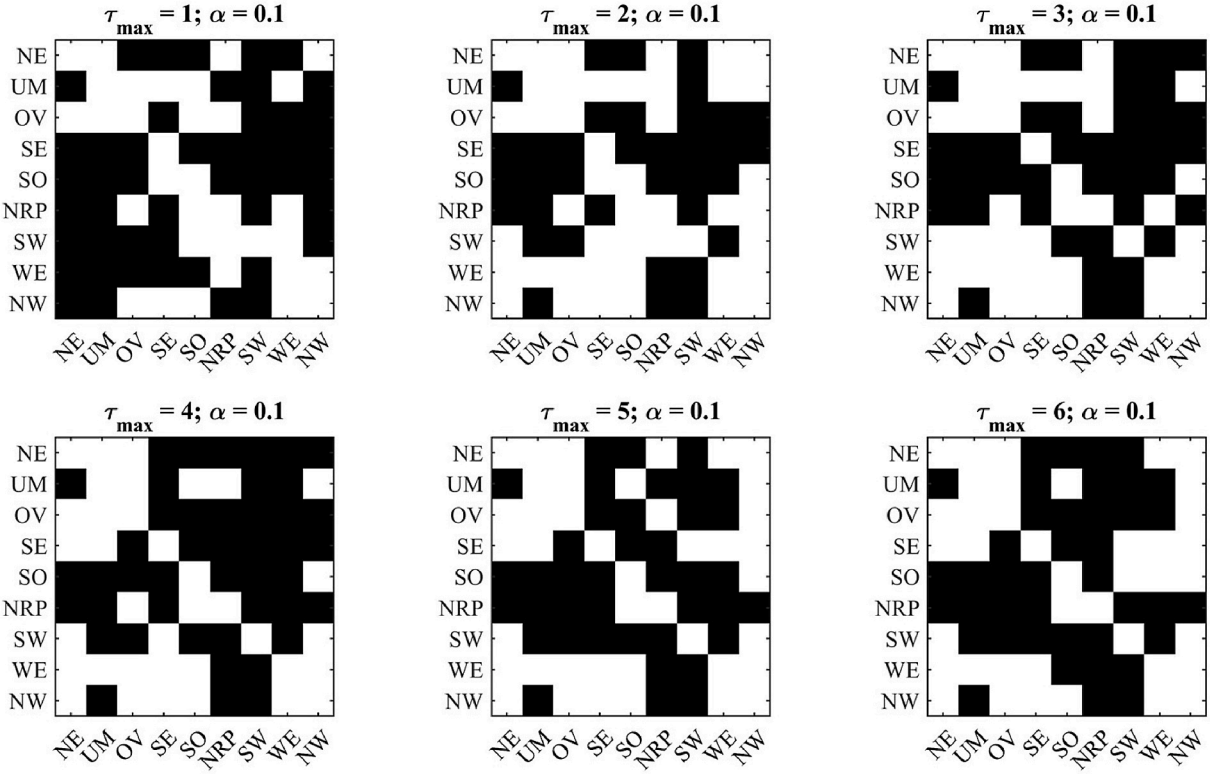

Fig. A2. Same with Fig. A1, but with different significance level $\alpha = 0.1$.

References

Ancona, N., Marinazzo, D., Stramaglia, S., 2004. Radial basis function approach to nonlinear Granger causality of time series. Phys. Rev. 70 (5), 056221 https://doi.org/10.1103/PhysRevE.70.056221.

Arblaster, J.M., Alexander, L.V., 2012. The impact of the El Niño-Southern Oscillation on maximum temperature extremes. Geophys. Res. Lett. 39 (20), L20702 https://doi.org/10.1029/2012GL053409.

Boers, N., Goswami, B., Rheinwalt, A., Bookhagen, B., Hoskins, B., Kurths, J., 2019. Complex networks reveal global pattern of extreme-rainfall teleconnections. Nature 566, 373–377. https://doi.org/10.1038/s41586-018-0872-x.

Charney, J.G., DeVore, J.G., 1979. Multiple flow equilibria in the atmosphere and blocking. J. Atmos. Sci. 36 (7), 1205–1216. https://doi.org/10.1175/1520-0469(1979)036<1205:MFEITA>2.0.CO. ;2.

Ding, M., Grebogi, C., Ott, E., Sauer, T., Yorke, J.A., 1993. Plateau onset for correlation dimension: when does it occur? Phys. Rev. Lett. 70, 3872–3875. https://doi.org/10.1103/PhysRevLett.70.3872.

Fan, J., Meng, J., Ludescher, J., Chen, X., Ashkenazy, Y., Kurths, J., et al., 2020. Statistical physics approaches to the complex Earth system. Phys. Rep. https://doi.org/10.1016/j.physrep.2020.09.005 (in press).

Fitzpatrick, M.C., Dunn, R.R., 2019. Contemporary climatic analogs for 540 North American urban areas in the late 21st century. Nat. Commun. 10, 614–617. https://doi.org/10.1038/s41467-019-08540-3.

Gershunov, A., Barnett, T.P., 1998. Interdecadal modulation of ENSO teleconnections. Bull. Am. Meteorol. Soc. 79 (12), 2715–2725. https://doi.org/10.1175/1520-0477(1998)079<2715:IMOET>2.0.CO. ;2.

Ghil, M., Lucarini, V., 2020. The physics of climate variability and climate change. Rev. Mod. Phys. 92 (3), 035002 https://doi.org/10.1103/RevModPhys.92.035002.

Good, P., Lowe, J.A., Andrews, T., Wiltshire, A., Chadwick, R., Ridley, J.K., Menary, M. B., Bouttes, N., Dufresne, J.L., Gregory, J.M., Schaller, N., Shiogama, H., 2015. Nonlinear regional warming with increasing CO_2 concentrations. Nat. Clim. Change 5, 138–142. https://doi.org/10.1038/nclimate2498.

Granger, C.W., 1969. Investigating causal relations by econometric models and cross-spectral methods. Econometrica 37, 424–438 https://doi.org/1912791.

Grassberger, P., Procaccia, I., 1983. Characterization of strange attractors. Phys. Rev. Lett. 50 (5), 346–349. https://doi.org/10.1103/PhysRevLett.50.346.

Grassberger, P., Procaccia, I., 2004. Measuring the strangeness of strange attractors. In: Hunt, B.R., Li, T.Y., Kennedy, J.A., Nusse, H.E. (Eds.), The Theory of Chaotic Attractors. Springer, New York, NY. https://doi.org/10.1007/978-0-387-21830-4_12.

Hall, A., 2004. The role of surface albedo feedback in climate. J. Clim. 17, 1550–1568. https://doi.org/10.1175/1520-0442(2004)017<1550:TROSAF>2.0.CO, 2.

Handorf, D., Jaiser, R., Dethloff, K., Rinke, A., Cohen, J., 2015. Impacts of Arctic sea ice and continental snow cover changes on atmospheric winter teleconnections. Geophys. Res. Lett. 42 (7), 2367–2377. https://doi.org/10.1002/2015GL063203.

Harris, I., Osborn, T.J., Jones, P., Lister, D., 2020. Version 4 of the CRU TS monthly high-resolution gridded multivariate climate dataset. Sci. Data 7 (1), 109. https://doi.org/10.1038/s41597-020-0453-3.

Huang, N.E., Shen, Z., Long, S.R., Wu, M.C., Shih, H.H., Zheng, Q., Yen, N.-C., Tung, C.C., Liu, H.H., 1998. The empirical mode decomposition and the Hilbert spectrum for nonlinear and non-stationary time series analysis. Proceedings of the Royal Society of London. Series A: Math. Phys. Eng. Sci. 454, 903–995. https://doi.org/10.1098/rspa.1998.0193, 1971.

Huang, Y., Kleindessner, M., Munishkin, A., Varshney, D., Guo, P., Wang, J., 2021. Benchmarking of data-driven causality discovery approaches in the interactions of Arctic sea ice and atmosphere. Frontiers in Big Data 4. https://doi.org/10.3389/fdata.2021.642182.

Ishizaki, Y., Shiogama, H., Emori, S., Yokohata, T., Nozawa, T., Ogura, T., Abe, M., Yoshimori, M., Takahashi, K., 2012. Temperature scaling pattern dependence on representative concentration pathway emission scenarios. Clim. Change 112, 535–546. https://doi.org/10.1007/s10584-012-0430-8.

Jiang, J.-J., Huang, Z.-G., Huang, L., Liu, H., Lai, Y.-C., 2016. Directed dynamical influence is more detectable with noise. Sci. Rep. 6 (1), 24088 https://doi.org/10.1038/srep24088.

Kantz, H., Schreiber, T., 1997. Nonlinear Time Series Analysis. Cambridge University Press.

Karl, T.R., Koscielny, A.J., 1982. Drought in the United States: 1895–1981. J. Climatol. 2 (4), 313–329. https://doi.org/10.1002/joc.3370020402.

Kenyon, J., Hegerl, G.C., 2008. Influence of modes of climate variability on global temperature extremes. J. Clim. 21 (15), 3872–3889. https://doi.org/10.1175/2008JCLI2125.1.

Konapala, G., Mishra, A., 2017. Review of complex networks application in hydroclimatic extremes with an implementation to characterize spatio-temporal drought propagation in continental USA. J. Hydrol. 555, 600–620. https://doi.org/10.1016/j.jhydrol.2017.10.033.

Lai, Y.-C., Ye, N., 2003. Recent developments in chaotic time series analysis. Int. J. Bifurcation Chaos 13 (6), 1383–1422. https://doi.org/10.1142/S0218127403007308.

Lau, N.-C., Nath, M.J., 2012. A model study of heat waves over north America: meteorological Aspects and Projections for the Twenty-First Century. J. Clim. 25 (14), 4761–4784. https://doi.org/10.1175/JCLI-D-11-00575.1.

Leng, S., Ma, H., Kurths, J., Lai, Y.-C., Lin, W., Aihara, K., Chen, L., 2020. Partial cross mapping eliminates indirect causal influences. Nat. Commun. 11 (1), 2632. https://doi.org/10.1038/s41467-020-16238-0.

Matsueda, M., 2011. Predictability of Euro-Russian blocking in summer of 2010. Geophys. Res. Lett. 38 (6) https://doi.org/10.1029/2010GL046557.

McCann, K., Hastings, A., Huxel, G.R., 1998. Weak trophic interactions and the balance of nature. Nature 395 (6704), 794–798. https://doi.org/10.1038/27427.

McGraw, M.C., Barnes, E.A., 2018. Memory Matters: a case for Granger causality in climate variability studies. J. Clim. 31 (8), 3289–3300. https://doi.org/10.1175/JCLI-D-17-0334.1.

Moran, P.a.P., 1953. The statistical analysis of the Canadian Lynx cycle. Aust. J. Zool. 1 (3), 291–298. https://doi.org/10.1071/zo9530291.

Namias, J., 1983. Some causes of United States drought. J. Appl. Meteorol. Climatol. 22 (1), 30–39. https://doi.org/10.1175/1520-0450(1983)022<0030:SCOUSD>2.0.CO. ;2.

Ombadi, M., Nguyen, P., Sorooshian, S., Hsu, K., 2020. Evaluation of methods for causal discovery in hydrometeorological systems. Water Resour. Res. 56 (7), e2020WR027251 https://doi.org/10.1029/2020WR027251.

Perkins, S.E., 2015. A review on the scientific understanding of heatwaves—their measurement, driving mechanisms, and changes at the global scale. Atmos. Res. 164 (165), 242–267. https://doi.org/10.1016/j.atmosres.2015.05.014.

Runge, J., Petoukhov, V., Donges, J.F., Hlinka, J., Jajcay, N., Vejmelka, M., et al., 2015. Identifying causal gateways and mediators in complex spatio-temporal systems. Nat. Commun. 6 (1), 8502. https://doi.org/10.1038/ncomms9502.

Runge, J., Nowack, P., Kretschmer, M., Flaxman, S., Sejdinovic, D., 2019. Detecting and quantifying causal associations in large nonlinear time series datasets. Sci. Adv. 5 (11), eaau4996 https://doi.org/10.1126/sciadv.aau4996.

Shi, H., Zhao, Y., Liu, S., Cai, H., Zhou, Z., 2022. A new perspective on drought propagation: causality. Geophys. Res. Lett. 49 (2), e2021GL096758 https://doi.org/10.1029/2021GL096758.

Silva, F.N., Vega-Oliveros, D.A., Yan, X., Flammini, A., Menczer, F., Radicchi, F., et al., 2021. Detecting climate teleconnections with Granger causality. Geophys. Res. Lett. 48 (18), e2021GL094707 https://doi.org/10.1029/2021GL094707.

Sugihara, G., May, R.M., 1990. Nonlinear forecasting as a way of distinguishing chaos from measurement error in time series. Nature 344 (6268), 734–741. https://doi.org/10.1038/344734a0.

Sugihara, G., May, R., Ye, H., Hsieh, C.-H., Deyle, E., Fogarty, M., Munch, S., 2012. Detecting causality in complex ecosystems. Science 338 (6106), 496–500. https://doi.org/10.1126/science.1227079.

Takens, F., 1981. Detecting strange attractors in fluid turbulence. In: Rand, D., Young, L. S. (Eds.), Dynamical Systems and Turbulence, vol. 898. Springer-Verlag, Berlin, pp. 366–381. https://doi.org/10.1007/BFb0091924.

Tsonis, A.A., Roebber, P.J., 2004. The architecture of the climate network. Physica A 333, 497–504. https://doi.org/10.1016/j.physa.2003.10.045.

van Nes, E.H., Scheffer, M., Brovkin, V., Lenton, T.M., Ye, H., Deyle, E., Sugihara, G., 2015. Causal feedbacks in climate change. Nat. Clim. Change 5 (5), 445–448. https://doi.org/10.1038/nclimate2568.

Walsh, J.E., Richman, M.B., Allen, D.W., 1982. Spatial coherence of monthly precipitation in the United States. Mon. Weather Rev. 110 (4), 272–286. https://doi.org/10.1175/1520-0493(1982)110<0272:SCOMPI>2.0.CO. ;2.

Wang, Z.H., 2021. Compound environmental impact of urban mitigation strategies: Co-benefits, trade-offs, and unintended consequence. Sustain. Cities Soc. 75, 103284 https://doi.org/10.1016/j.scs.2021.103284.

Wang, Z.H., 2022. Reconceptualizing urban heat island: beyond the urban-rural dichotomy. Sustain. Cities Soc. 77, 103581 https://doi.org/10.1016/j.scs.2021.103581.

Wang, C., Wang, Z.H., 2020. A network-based toolkit for evaluation and intercomparison of weather prediction and climate modeling. J. Environ. Manag. 268, 110709 https://doi.org/10.1016/j.jenvman.2020.110709.

Wang, Y., Gozolchiani, A., Ashkenazy, Y., Berezin, Y., Guez, O., Havlin, S., 2013. Dominant imprint of Rossby waves in the climate network. Phys. Rev. Lett. 111 (13), 138501 https://doi.org/10.1103/PhysRevLett.111.138501.

Wang, Y., Yang, J., Chen, Y., De Maeyer, P., Li, Z., Duan, W., 2018. Detecting the causal effect of soil moisture on precipitation using convergent cross mapping. Sci. Rep. 8 (1), 12171 https://doi.org/10.1038/s41598-018-30669-2.

Wang, C., Wang, Z.H., Li, Q., 2020a. Emergence of urban clustering among U.S. cities under environmental stressors. Sustain. Cities Soc. 63, 102481 https://doi.org/10.1016/j.scs.2020.102481.

Wang, C., Wang, Z.H., Sun, L., 2020b. Early-warning signals for critical temperature transitions. Geophys. Res. Lett. 47, e2020GL088503 https://doi.org/10.1029/2020GL088503.

Wang, Z.H., Wang, C., Yang, X., 2021. Dynamic synchronization of extreme heat in complex climate networks in the contiguous United States. Urban Clim. 38, 100909 https://doi.org/10.1016/j.uclim.2021.100909.

Yang, X., Wang, Z.H., Wang, C., 2022. Critical transitions in the hydrological system: early-warning signals and network analysis. Hydrol. Earth Syst. Sci. 26 (7), 1845–1856. https://doi.org/10.5194/hess-26-1845-2022.

Zhang, X., Wang, J., Zwiers, F.W., Groisman, P.Y., 2010. The Influence of large-scale climate variability on winter maximum daily precipitation over North America. J. Clim. 23 (11), 2902–2915. https://doi.org/10.1175/2010JCLI3249.1.